Inferring static elastic properties of fractures from flow measurements

Joseph Ho Yin Ma [,1], Qiaomu Qi [1], Yu Qiu [1,2], Yunyue Elita Li [1], and Arthur Cheng [1]*
[1] Department of Civil and Environmental Engineering, National University of Singapore
[2] Key Laboratory of Groundwater Resources and Environment, Jilin University

Summary

The roughness of fracture surfaces controls both the flow and elastic properties. While the aperture opening and its height controls the flow and transport properties, the contacted area and the stress-free surface determine the elastic properties. An implicit, and potentially complicated relation exists connecting these two properties. In this paper, we demonstrate that, with a fracture in a granite core, the static compressibility of the fracture can be estimated from the steady state flow measurements. We establish an empirical relation between the compression displacement and the effective pressure, based on numerical simulations of fluid-flow through the digitized fracture surface. The resulting empirical relation shows reasonable agreement compared with those presented in earlier literatures.

Introduction

Fractures act as major conductive paths for the geo-fluids, hence dominating the hydraulic behavior of the reservoir rocks. The connected fracture apertures provide the percolation passage through which fluid flows (e.g. Pyrak-Nolte et al., 2016). The size and distribution of the apertures dictate the hydraulic response of the fractured media (Unger and Maze, 1993; Ma et al., 2017). Characterizing the fractures plays a critical role in design and risk assessment of many subsurface engineering activities, such as hydrocarbon production, geothermal energy extraction, CO_2 sequestration and nuclear waste disposal.

On the other hand, the fracture asperities are connected via the rock matrix. The quantity and the spatial distribution of the asperities in contact determine the stiffness of the fracture, and further influence the static compressibility and the dynamic velocity of the fractured rock (Swan, 1983; Choi et al., 2014). Thus, stress-dependent fracture geometry alteration (i.e., the aperture and the asperity networks) implicitly defines the interdependence of the flow and the elastic properties. Such linkage provides an opportunity for integrating the flow and the seismic data for the fracture characterization (Kang et al., 2016) and the further geologic model building (Li et al., 2015).

Previous studies attempt to investigate the coupled flow-elastic behavior in rocks, some of which established model for estimating the reservoir permeability from the seismic scattering data (Brown and Fang, 2012). In reality, permeability of a fractured rock is usually difficult to be determined in-situ, especially in a field condition. Similarly, the estimation of fracture stiffness is not straight forward. Available methods include implicit calculation from static stress-closure relation (Goodman, 1976) or deduction from the dynamic pulse transmission experiments (Pyrak-Nolte et al., 1990). Nevertheless, these methods aim to obtain or estimate the fracture elasticity parameters from direct mechanical perspective, which might not be feasible to obtain in-situ.

In this work, we investigate the potential of directly inferring the fracture stiffness from the laboratory permeability measurements. We first measure the steady state permeability with increasing confining stress. Independently, we conduct the flow simulation based on the scanned fracture surface profile and apply with a series of normal displacement as the compression effect from stressing. By matching the measured and the simulated permeability at the different stresses, we obtain a stress-displacement relation. Finally, we compare the inferred static compressibility of the fractured rock with those reported of other rocks.

Methodology

We conducted this study based on a single fracture in a granite core of length L_x = 76 mm and diameter L_y = 35 mm. Steady state volumetric flow rate measurements were made under changing confining pressure from 5 MPa to 25 MPa with a fixed fluid pressure of 2 MPa. The fracture surfaces were then scanned for the topographies. The digital profiles obtained were in 0.2 mm resolution, as shown in Figure 1.

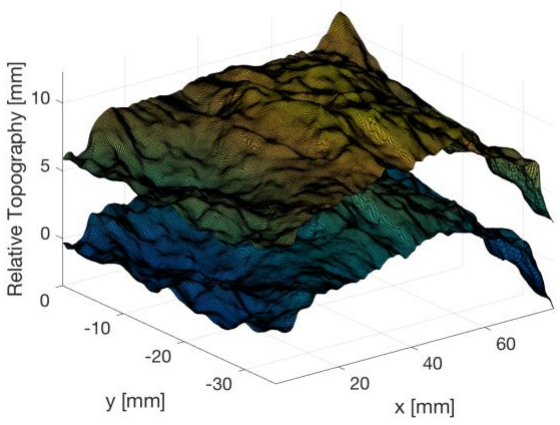

Figure 1: The digital profile of the granite core fracture surfaces.

With the high-resolution topography of the fracture surfaces, we deduced the equivalent semi-rough fracture model (Figure 2). This model provided simpler description of fracture surface roughness and compression, while preserving the aperture distribution information of the original rough surfaces. When there was no external stress, the flat upper surface was assumed to be in first contact with the lower rough surface. Compression of fracture surfaces was modelled by reducing the relative displacements between surfaces, i.e. the compression displacement d, by factors of standard deviation of the resultant rough surface height σ, with no intersection between the surfaces.

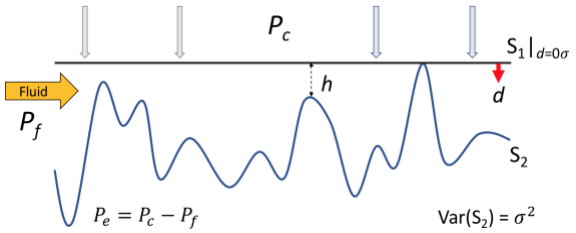

Figure 2: A schematic illustration of the semi-rough fracture model and the pressure components involved.

We simulated the incompressible fluid flow in the equivalent semi-rough fracture under different compression levels with Darcy's Law (Equation 1) under the corresponding boundary conditions. The average flow flux $\boldsymbol{q} = (q_x, q_y)$ was related to the permeability k, dynamic fluid viscosity μ and the fluid pressure gradient ∇P_f. By approximating the surfaces to be locally parallel, the local permeability relates to the aperture height h by $k = h^2/12$.

$$\boldsymbol{q} = -\frac{k}{\mu}\nabla P_f \tag{1}$$

From the simulated flow flux in fracture, the volumetric flow rate Q across the fracture was calculated. We translate the volumetric flow rate to permeability, which is a more commonly used representation of the flow capability. We first found the hydraulic aperture from the inverse of the cubic Darcy's law (Equation 2). The effective permeability $\bar{k}$ can be easily calculated using Equation 3 since the hydraulic aperture could also understood as the aperture height of a parallel plate fracture with equivalent permeability. Same principle was applied to experimental data to calculate the measured permeability.

$$h_{\mathrm{hydraulic}} = \left(\frac{12\mu Q L_x}{L_y \Delta P_f}\right)^{1/3} \tag{2}$$

$$\bar{k} = h_{\mathrm{hydraulic}}^2/12 \tag{3}$$

By matching the normalized permeability change under increasing confining pressure (from experiment measurements) and simulated permeability change under increasing compression displacement (from flow simulations), we obtained an estimate to relate effective pressure with the compression displacement of the fracture. This allowed an inversion for an empirical relation between these quantities. We fit the result with a parametric relation given in Swan (1983) (Equation 4), which suggested that the compression displacement in rough fractures was related to the logarithmic of the effective pressure. The inverted compression displacement-effective pressure relation from flow measurements further enabled the understanding of fracture elastic properties. For instance, we examined the fracture compliance S from the relative changes in strain ϵ against effective pressure (Equation 5). Finally, we compared the inverted fracture incompressibility γ, defined as inverse of the difference between fracture compliance S and background compliance S_{bg} (Equation 6), in this granite core with the incompressibility of other cracked rocks presented in earlier literatures.

$$d = A + B\ln P_e \tag{4}$$

$$S = \frac{\partial \epsilon}{\partial P} \tag{5}$$

$$\gamma = \left(S - S_{\mathrm{bg}}\right)^{-1} \tag{6}$$

Results

Figure 3 shows the relation between measured volumetric flow rate and confining pressure of the granite core. It shows that the volumetric flow rate decreases almost log-linearly with increasing confining pressure. It could be seen from numerical flow simulation, with examples illustrated in Figure 4, that increasing compression on the fracture increases the contact area and therefore the flows are concentrated into the remaining channels. The reduction in aperture height under compression results in less permeable fractures and thus both the local flow flux and overall volumetric flow rate are decreased.

We invert for the relation between confining pressure and the magnitude of compression (in terms of σ) in the fracture by matching the normalized fracture permeability obtained from experimental measurements and numerical simulations (Figure 5). The results are presented in the two vertical axes of Figure 5, with $\sigma = 2.04 \times 10^{-4}$ m. Since all flow measurements are made at same fluid pressure (2 MPa), the relation can be directly translated into effective pressure against compression displacement. It is suggested from the inverted results that within the effective pressure range of 3 to 23 MPa (left axis), the fracture is compressed from 0.31

mm to 0.57 mm (right axis). The compression magnitudes are less than 1.6 % of the core diameter. The inverted compression displacement is nearly linear against confine ng pressure in log-log scale., which provides the confidence of using Equation 4 for construction of our empirical relation.

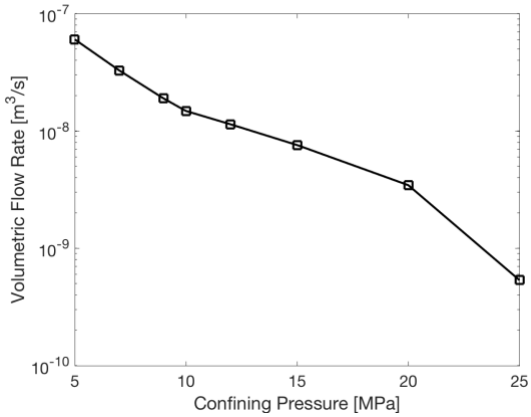

Figure 3: The measured volumetric flow rate across granite fracture under different confining pressure.

(a)

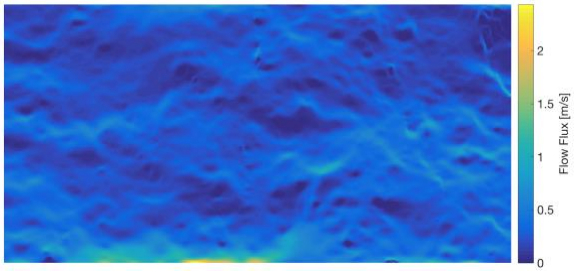

(b)

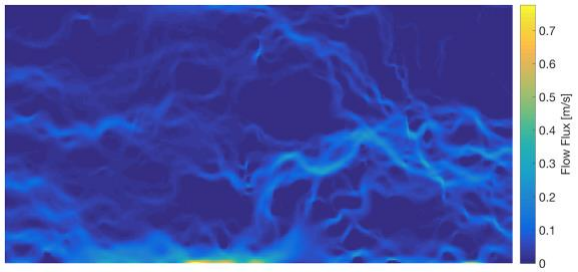

Figure 4: The simulated averaged flow flux field in the granite fracture under compression displacement of (a) 1.5 σ and (b) 2.5 σ.

The empirical relation fitted from data is given by:

$$d = -1.48 \times 10^{-3} + 1.20 \times 10^{-4} \ln P_e \ , \qquad (7)$$

which is shown in the outer plot of Figure 6. It shows that the proposed parametric relation is in high level of agreement with the permeability-inverted data points. From the inversion results based on regression fitting, it is suggested that an effective pressure of 3 MPa is capable to compress the fracture by 0.3 mm, while it would require extra 30 MPa to further compress it by the same amount. We then estimate the fracture compliance from the fitted curve, as shown in the inner plot of Figure 6.

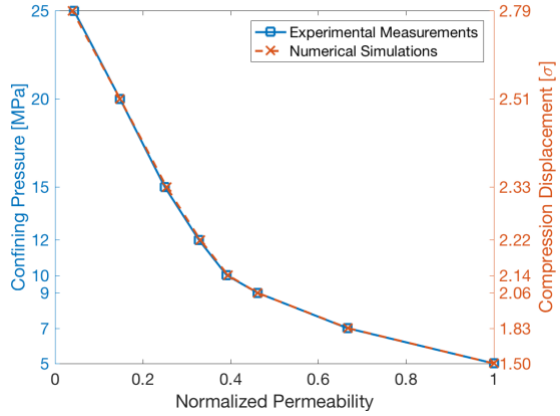

Figure 5: Normalized Permeability as a function of confining pressure from experimental measurements and numerical simulations respectively.

The inverted static fracture compliance drops significantly for effective pressure less than 2 MPa while remained in the same order of magnitude under higher effective pressure. It is also suggested in our experimental effective pressure range, the compliance of the granite core is of an order of 10^{-10} Pa^{-1} . Finally, we investigate the fracture incompressibility, which is defined by the inverse of the difference between core compliance and background compliance. Assuming a Young's modulus E of 60 GPa, a Poisson ratio ν of 0.25 and comparatively negligible porosity for the granite core, the core would have a bulk modulus of $E/3(1-2\nu)$ = 40 GPa. The background compliance of the granite core could be calculated from the reciprocal of the bulk modulus (stiffness). The inverted fracture incompressibility against effective pressure is shown in Figure 7, together with previously published results on other types of rocks. It is observed that the inverted fracture incompressibility is noticeably lower than other rocks. Below an effective pressure of 60 MPa, the fracture incompressibility is almost linearly related to effective pressure.

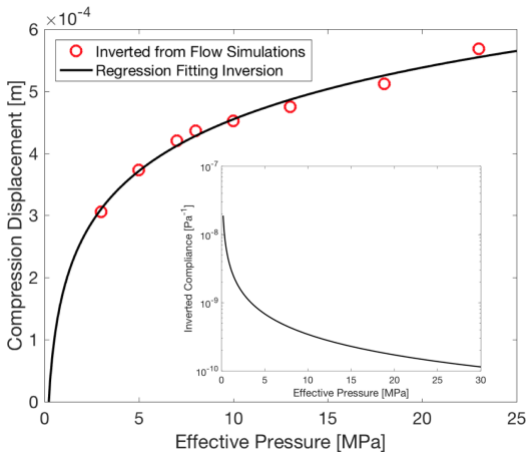

Figure 6: The relation between fracture compression displacement and effective pressure inferred from flow measurements (outer plot), with the inverted fracture compliance (inner plot).

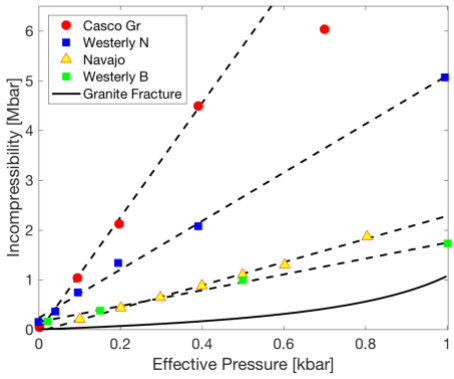

Figure 7: The inverted granite fracture incompressibility from flow measurements (in solid line), compared with other cracked rocks, modified from Walsh and Grosenbaugh [1979].

Discussion

From the changes of permeability under varying confining pressure, an empirical relationship between confining pressure and standard deviation of aperture heights can be established, as shown above. If the topography of both rough surfaces is known, we could then further estimate the compression displacement, and thus the strain on fracture, under various confining pressure. However, in reality, especially in subsurface reservoirs, it would be almost impossible to obtain the surface topographies. Nevertheless, Ma et al. (2017) illustrated that various aperture distribution could result in fractures of similar flow behavior, and that a unique set of statistical parameters (autocorrelation length and height variance of an equivalent semi-rough fracture model) characterization could be obtained by examining fracture flow properties under various compression states. These results suggest that flow properties in stressed rough fractures might be sufficient to provide an estimation to its static elastic properties.

The linear incompressibility trend obtained for low effective pressure is consistent with that suggested by Walsh and Gorensenbaugh (1979). Our inverted incompressibility for granite fracture is shown to be lower compared to that in other rocks, which indicates a softer background granite medium. The presence of fracture would lead to additional stress-free areas compare to rocks with typical cracks. Therefore, stiffness might be significantly reduced.

Nevertheless, the inverted incompressibility could be slightly overestimated. As the slope of lines in Figure 8 is suggested to be proportional to the apparent surface area per unit volume times the standard deviation of the aperture, it could be affected by the mechanism which fracture is compressed. In our forward modelling of flow simulations, elastic deformation of fracture under stressing (Timoshenko and Goodier, 1951; Unger and Mase, 1993) is not considered. Such considerations, which are deemed to be more realistic, would suggest a smaller apparent surface area since it includes the reversed surface displacement in uncontacted regions. Thus, the actual apparent surface area might be lower than expected which would give a gentler slope on incompressibility against pressure.

Conclusion

In this study, we demonstrate the potential of inverting fracture static elasticity parameters from steady state flow measurements. An empirical relation between fracture compression displacement and confining pressure has been obtained from matching the experimental and simulated permeability under pressure. The inverted relation suggests the static compressibility of the fractured granite core is comparable to those presented in earlier literatures. The results imply that fluid flow measurements could provide certain insights and information about the static elasticity behavior of a fracture.

Acknowledgements

The authors acknowledge the EDB Petroleum Engineering Professorship for their financial support. Dr. Yunyue Elita Li is funded by MOE Tier-1 Grant R-302-000-165-133 and R-302-000-182-114. The authors also thank Key Laboratory of Groundwater Resources and Environment at Jilin University for their contribution in the experimental measurements.

References

Brown, S., and Fang, X., 2012, Fluid flow property estimation from seismic scattering data: In *SEG Technical Program Expanded Abstracts 2012*, 1-6.

Choi, M. K., Bobet, A., and Pyrak-Nolte, L. J., 2014, The effect of surface roughness and mixed-mode loading on the stiffness ratio κ_x/κ_z for fractures: *Geophysics*, ***79***(5), D319-D331.

Goodman, R. E., 1976, *Methods of geological engineering in discontinuous rocks*.

Kang, P. K., Zheng, Y., Fang, X., Wojcik, R., McLaughlin, D., Brown, S., Fehler M.C., Burns, D.R., and Juanes, R., 2016, Sequential approach to joint flow-seismic inversion for improved characterization of fractured media: *Water Resources Research*, ***52***(2), 903-919.

Li, Y., Biondi, B., Mavko, G., and Nichols, D., 2015, Integrated VTI Model Building with Seismic, Geological and Rock Physics Data: In *77th EAGE Conference and Exhibition 2015*.

Ma, J. H. Y., Li, Y.E., and Cheng, A., 2017, The effects of aperture distribution and compression on transport properties in rock fractures: In *SEG Technical Program Expanded Abstracts 2017*, 3945-3949.

Pyrak-Nolte, L. J., Myer, L. R., and Cook, N. G., 1990, Transmission of seismic waves across single natural fractures: *Journal of Geophysical Research: Solid Earth*, ***95***(B6), 8617-8638.

Pyrak-Nolte, L. J., and Morris, J. P., 2000, Single fractures under normal stress: The relation between fracture specific stiffness and fluid flow: *International Journal of Rock Mechanics and Mining Sciences*, ***37***(1-2), 245-262.

Pyrak-Nolte, L. J., and Nolte, D. D., 2016, Approaching a universal scaling relationship between fracture stiffness and fluid flow: *Nature communications*, ***7***, 10663.

Swan, G., 1983, Determination of stiffness and other joint properties from roughness measurements: *Rock Mechanics and Rock Engineering*, ***16***(1), 19-38.

Timoshenko, S.P., and Goodier, J. N., 1951, *Theory of Elasticity*, McGraw-Hill book Company.

Walsh, J. B., and Grosenbaugh, M. A., 1979, A new model for analyzing the effect of fractures on compressibility: *Journal of Geophysical Research: Solid Earth*, ***84***(B7), 3532-3536.

Unger, A. J. A., and Mase, C. W., 1993, Numerical study of the hydromechanical behavior of two rough fracture surfaces in contact: *Water Resources Research*, ***29*** (7), 2101-2114.